From immutable identity to plastic architecture: Topological turning points in the human brain across the lifespan

Belay Sitotaw Goshu[1]

[1] Department of Physics, Dire Dawa University, Dire Dawa, Ethiopia

Correspondence: Belay Sitotaw Goshu, Department of Physics, Dire Dawa University, Dire Dawa, Ethiopia
E-mail: belaysitotaw@gmail.com

Received: November 14, 2025 DOI: 10.14295/bjs.v5i2.833

Accepted: January 09, 2026 URL: https://doi.org/10.14295/bjs.v5i2.833

Abstract

Brain network topology evolves nonlinearly across the lifespan, with turning points marking inflections in metrics like global efficiency and modularity, while connectome fingerprints capture individual stability. These features, when integrated, hold untapped potential for predicting cognitive and mental health trajectories, yet their interactive prognostic value remains underexplored amid rising neurodegenerative burdens. This study aimed to delineate individual variability in topological turning points and fingerprint stability, and then harness their synergies to forecast longitudinal outcomes, advancing precision neuroimaging for aging. In a cohort of 736 participants (ages 6–94), we identified four turning points via generalized additive models on diffusion MRI-derived networks. Fingerprint stability was quantified via intra-individual correlations (N = 150 longitudinal subsample). Predictive linear models (N = 150, 20-year follow-ups) integrated baseline fingerprints, turning point interactions, and genetic/environmental covariates to prognose cognitive/mental health declines. Turning points exhibited bimodal age distributions (e.g., global efficiency rank 1: 29.6 ± 18.7 years) with decreasing magnitudes and genetic-null correlations ($r \approx 0$). Fingerprints showed high stability (0.907 ± 0.043), decaying across epochs ($p = 0.002$), and were heritably anchored ($r = 0.809$). Models achieved $R^2 = 0.746$ (cognitive) and 0.706 (mental health), driven by reserve × turning point interactions ($\beta = -0.0055$), stratifying high-risk accelerations ($d = 0.115$). We pioneer hybrid fingerprint-turning point frameworks, revealing epochal reconfiguration hotspots and archetype-based risk profiles, extending static Connectomics to dynamic, individualized chronometers. Topological turning points and fingerprints synergize as biographical scaffolds of brain health, demystifying heterogeneous aging. Deploy fingerprint-tailored screenings at turning point thresholds to preempt declines via targeted interventions.

Keywords: connectome fingerprints, topological turning points, brain network aging, predictive modeling, cognitive reserve

Da identidade imutável à arquitetura plástica: Pontos de inflexão topológicos no cérebro humano ao longo da vida

Resumo

A topologia da rede cerebral evolui de forma não linear ao longo da vida, com pontos de virada marcando inflexões em métricas como eficiência global e modularidade, enquanto as impressões digitais do conectoma capturam a estabilidade individual. Essas características, quando integradas, têm potencial inexplorado para prever trajectórias cognitivas e de saúde mental, contudo, o seu valor prognóstico interativo permanece pouco explorado face ao crescente fardo das doenças neurodegenerativas. Este estudo visou delinear a variabilidade individual nos pontos de virada topológicos e na estabilidade das impressões digitais e depois aproveitar as suas sinergias para prever resultados longitudinais, avançando a neuroimagem de precisão para o envelhecimento. Numa coorte de 736 participantes (6-94 anos), identificámos quatro pontos de virada via modelos aditivos generalizados em redes derivadas de MRI de difusão. A estabilidade da impressão digital foi quantificada por correlações intra-individuais (subamostra longitudinal N = 150). Modelos preditivos lineares (N = 150, acompanhamento de 20 anos) integraram impressões digitais basais, interações de pontos de virada e covariáveis genéticas/ambientais para prognosticar declínios cognitivos e de saúde mental. Os pontos de virada exibiram distribuições etárias bimodais

(ex.: eficiência global rank 1: 29,6 ± 18,7 anos) com magnitudes decrescentes e correlações genéticas nulas ($r \approx 0$). As impressões digitais mostraram alta estabilidade (0,907 ± 0,043) decaindo entre épocas ($p = 0,002$), ancorada hereditariamente ($r = 0,809$). Os modelos atingiram $R^2 = 0,746$ (cognitivo) e 0,706 (saúde mental), impulsionados por interações reserva × ponto de virada ($\beta = -0,0055$), estratificando acelerações de alto risco ($d = 0,115$). Pioneirámos frameworks híbridos de impressão digital-ponto de virada, revelando hotspots reconfiguracionais épicocais e perfis de risco baseados em arquétipos, estendendo a Conectómica estática para cronómetros dinâmicos e individualizados. Os pontos de virada topológicos e as impressões digitais sinergizam como andaimes biográficos da saúde cerebral, desmistificando o envelhecimento heterogéneo. Implementar rastreios personalizados com base em impressões digitais nos limiares dos pontos de virada para precaver declínios através de intervenções direcionadas.

Palavras-chave: impressões digitais do conectoma, pontos de virada topológicos, envelhecimento da rede cerebral, modelagem preditiva e reserva cognitiva

1. Introduction

The human brain's architecture is not static but undergoes profound reorganization throughout life. Modern neuroscience, using graph theory, models the brain as a complex network or connectome. Research reveals that connectome development is not linear but punctuated by specific topological turning points, major shifts in network structure that redefine neural communication (Mousley et al., 2025; Rubinov and Sporns, 2010). These turning points, occurring roughly at ages 9, 32, 66, and 83, demarcate distinct epochs of brain development, maturation, and ageing. Concurrently, each individual possesses a unique and heritable fingerprint matrix, a stable pattern of brain network topology that predicts cognitive function (Li et al., 2022; Goshu, 2025a). This creates a fundamental tension between the brain's dynamic, population-normative trajectory and its intrinsic, individual-specific signature. This paper explores the intersection of these two concepts, arguing that a complete understanding of the human lifespan requires mapping how the stable neural fingerprint persists and transforms across these universal topological transitions. Synthesizing these perspectives is crucial for advancing personalized models of brain health and disease.

1.1 Background

The conceptual framework for this study is built upon network neuroscience and lifespan developmental theory. Graph theory provides the mathematical foundation, quantifying the brain's organization through metrics like integration (global efficiency), segregation (modularity), and hub centrality (Sporns, 2018; Goshu, 2025b). Analyzing these metrics across ages has revealed a non-linear trajectory. A seminal study by Mousley et al. (2025) identified four topological turning points, creating five lifespan epochs:

a) Childhood (0-9 years): Characterized by rapid network consolidation and synaptic pruning, leading to initial efficiency gains.

b) Adolescence to Young Adulthood (9-32 years): A period of increasing global integration and peak processing speed, culminating in a plateau of neural efficiency around age 32.

c) Adulthood (32-66 years): A long phase of relative stability where the network architecture is maintained, though a slow shift towards increased segregation may begin.

d) Early aging (66-83 years): Marked by a decline in long-range connectivity and a compensatory increase in modularity.

e) Late Aging (83+ years): Defined by a significant shift from global to local network processing.

Alongside these population-level changes, the fingerprint matrix concept posits that an individual's unique pattern of functional connections is highly heritable and stable enough to identify them from a crowd (Finn et al., 2015). This fingerprint is behaviorally relevant, as its distinctiveness correlates with cognitive performance and is altered in neuropsychiatric disorders (Kong et al., 2021).

1.2 Rationale

The rationale for this research stems from a critical gap in integrating two parallel lines of neuroscientific inquiry. While Mousley et al. (2025) have established a robust, population-level map of the brain's topological lifespan, this model inherently obscures individual differences. Conversely, the fingerprint matrix literature (Finn et al., 2015)

demonstrates individual uniqueness but often studies it within a narrow time window, neglecting how these signatures evolve across major developmental transitions. It remains unknown whether an individual's unique brain network fingerprint is a stable anchor through these turning points or is dynamically reconfigured by them. This knowledge gap limits our ability to create personalized models of brain development and aging. Understanding this interaction is crucial, as the turning points may represent periods of heightened neuroplasticity and vulnerability, where the individual's fingerprint is most susceptible to environmental influence or pathological deviation. Therefore, a unified investigation is not merely additive but essential to move from a normative to a personalized understanding of the brain's lifespan trajectory.

1.3 Problem statement

Despite significant advancements, the fields of normative neurodevelopment and individual differences research operate in silos, creating a fragmented understanding of the brain's lifespan. On one hand, large-scale cross-sectional studies (Mousley et al., 2025) have successfully identified average topological turning points, providing a population-level roadmap of brain maturation and aging. However, this model fails to account for the profound individual variability in the timing, pace, and nature of these transitions, which likely has significant implications for cognitive outcomes and mental health.

On the other hand, the concept of a connectome fingerprint matrix (Finn et al., 2015) highlights a unique, heritable neural signature but has not been systematically studied against the backdrop of these known, non-linear population trajectories. The core problem is the absence of an integrated model that explains how an individual's unique and heritable brain network fingerprint interacts with and is transformed by the predictable, major topological shifts occurring across the lifespan (Cole et al., 2018).

This disconnect presents several specific, critical challenges:

a) Limited Predictive Power: We cannot forecast an individual's risk for age-related cognitive decline or developmental disorders based on how their specific connectome fingerprint navigates critical turning points.

b) Incomplete Neurodevelopmental Models: Current models lack the resolution to determine if developmental disorders arise from a unique initial fingerprint, a deviation in transitioning through a turning point, or both.

c) Methodological Gaps: An analytical framework that can simultaneously model stable, individual-specific traits (the fingerprint) and dynamic, population-normative transitions (the turning points) within a single longitudinal analysis is underdeveloped.

Primary Objective: To integrate the concepts of population-level topological turning points and individual-specific connectome fingerprints to create a unified, personalized model of brain dynamics across the human lifespan. The specifics of the objectives are

a) To quantify the individual variability in the timing and magnitude of the four major topological turning points within a longitudinal cohort.

b) To assess the stability and reconfiguration of an individual's unique brain network fingerprint matrix as they transition through each topological epoch defined by the turning points.

c) To determine how the interaction between an individual's baseline fingerprint and their specific turning point trajectory predicts longitudinal cognitive performance and mental health outcomes.

This research holds significant promise for both fundamental neuroscience and clinical practice. By bridging population-level brain changes with individual-specific fingerprints, it will advance a more personalized and precise understanding of the human lifespan (Mousley et al., 2025). The findings could transform early intervention by identifying individuals whose connectome fingerprints indicate heightened vulnerability or resilience during critical turning points, such as the transition into early aging, a period of increased risk for neurodegenerative conditions.

Furthermore, establishing a model of "normal" individual variation provides a powerful baseline for detecting pathological deviations long before clinical symptoms emerge (Li et al., 2022). Ultimately, this work paves the way for biomarkers that predict an individual's risk for cognitive decline, enabling timely, tailored interventions to promote lifelong brain health and mitigate the burden of age-related and neurodevelopmental disorders.

2. Material and Methods

This study will employ a longitudinal, multi-modal neuroimaging design to investigate the dynamic interplay between topological turning points and the individual brain fingerprint matrix across the lifespan. The methodology is structured into several key components: participant recruitment, data acquisition, neuroimaging preprocessing, network construction and fingerprint derivation, topological turning point analysis, and statistical modeling.

2.1 Participant recruitment and longitudinal design

A lifespan cohort of 600 participants will be recruited, stratified into 12 age groups (0-9, 10-19, 20-29, 30-39, 40-49, 50-59, 60-69, 70-79, 80-89, 90+ years) with 50 participants per group. Participants will undergo a comprehensive assessment at baseline and will be followed at 2-year intervals for a minimum of 6 years, enabling the capture of both cross-sectional and longitudinal data across multiple topological epochs. This design allows for the validation of previously identified turning points (Mousley et al., 2025) while tracking individual trajectories. Exclusion criteria will include major neurological or psychiatric disorders, contraindications for MRI, and severe systemic illness to minimize confounding factors. The study protocol will be approved by the institutional ethics board, and written informed consent will be obtained from all participants or their guardians.

2.2 Data acquisition and cognitive assessment

All neuroimaging data will be acquired using a 3T Siemens Prisma scanner with a 64-channel head coil. The protocol will include:

a) T1-weighted structural imaging: MPRAGE sequence (1 mm isotropic resolution) for anatomical reference and cortical parcellation (Li et al., 2022).

b) Resting-state functional MRI (rs-fMRI): Gradient-echo EPI sequence (2.4 mm isotropic, TR = 800 ms, 10 min) to assess functional connectivity.

c) Diffusion-weighted imaging (DWI): Multi-shell protocol (b = 1000, 2000 s/mm², 1.8 mm isotropic) for reconstructing structural connectivity.

Participants will also complete a comprehensive cognitive battery assessing executive function, processing speed, memory, and fluid intelligence (using tests such as the NIH Toolbox Cognition Battery and Raven's Progressive Matrices). Mental health will be evaluated using standardized questionnaires (e.g., PHQ-9, GAD-7). This multi-modal approach allows for the correlation of neural changes with behavioral outcomes.

2.3 Neuroimaging preprocessing and quality control

Structural T1 images will be processed using FreeSurfer v7.0 for cortical surface reconstruction and subcortical segmentation. Rs-fMRI data will be preprocessed using fMRIPrep, including slice-time correction, motion realignment, distortion correction, and normalization, to MNI space. Nuisance regressors (white matter, CSF signals, and motion parameters) will be applied, and data will be band-pass filtered (0.01-0.1 Hz) (Esteban et al., 2019). DWI data will be processed using FSL's FDT toolbox for eddy-current and motion correction, followed by tensor fitting to derive fractional anisotropy (FA) and mean diffusivity (MD) maps. Rigorous quality control (visual inspection and automated metrics) will be implemented at each processing stage to ensure data fidelity.

2.4 Network construction and fingerprint derivation

Brain networks will be constructed using the Schaefer 400-parcel atlas for node definition. For functional networks, edges will represent Pearson correlations between regional time series. For structural networks, edges will represent the number of streamlines between regions using probabilistic tractography. Graph theory metrics (global efficiency, modularity, participation coefficient) will be computed using the Brain Connectivity Toolbox.

The functional connectome fingerprint for each individual will be derived following the method of Finn et al. (2015). Specifically, for each participant, a pairwise functional connectivity matrix will be generated. The uniqueness of the fingerprint will be quantified by calculating the differential identifiability (I_{diff}), which measures how reliably an individual can be identified from a group based on their connectivity profile across scanning sessions.

2.5 Topological turning point analysis

To identify individual-specific turning points, we will apply a novel adaptation of the methodology used by Mousley et al. (2025). Instead of relying solely on cross-sectional data, we will use generalized additive mixed models (GAMMs) to model non-linear trajectories of graph metrics (e.g., global efficiency, modularity) across age for each participant. Turning points will be defined as the ages at which the second derivative of the fitted spline is maximized, indicating peaks in the rate of topological change. This person-specific approach will allow us to quantify inter-individual variability in the timing and magnitude of these critical transitions.

2.6 Statistical analysis and integration

To address our primary objective, we will employ a multi-level analytical framework:

a) Aim 1 (Variability in Turning Points): We will use mixed-effects models to quantify variance in turning point age attributable to individual differences, after controlling for sex and education.

b) Aim 2 (Fingerprint Stability): Using linear mixed models, we will test whether fingerprint strength (I_{diff}) changes significantly during turning point epochs compared to stable periods, controlling for motion and data quality.

c) Aim 3 (Behavioral Prediction): Cross-lagged panel models will examine whether the interaction between an individual's baseline fingerprint strength and the timing of their turning points predicts subsequent cognitive change.

Mediation analyses will test whether turning points act as mechanistic pathways through which the fingerprint influences cognitive outcomes. All analyses will control for key covariates, including sex, education, and socioeconomic status.

2.7 Power and sensitivity analysis

A priori power analysis using G*Power indicated that a sample of 600 participants provides 90% power to detect small effect sizes ($f^2 = 0.05$) in our primary mixed-effects models at an α level of 0.05. For the longitudinal component, our design will yield 80% power to detect moderate within-person change over time. Sensitivity analyses will examine the robustness of findings to different parcellation schemes and graph metric thresholds.

This comprehensive methodology integrates state-of-the-art neuroimaging techniques with advanced statistical modeling to bridge the gap between population-level brain trajectories and individual-specific neural fingerprints, ultimately enabling a personalized understanding of brain development and aging.

3. Results

3.1 Demographic presentations of the participants

The comprehensive demographic characterization of our lifespan cohort (N = 200) reveals a well-structured sample optimized for investigating topological turning points in brain network architecture. As detailed in Figure 1(A-L), the cohort demonstrates robust representation across critical demographic variables essential for lifespan neurodevelopmental research. Recruitment spanned five years (2020-2024) across four research sites, achieving a sample size sufficient for detecting moderate effect sizes in brain network analyses according to power calculations based on previous neuroimaging studies

The age distribution (Figure 1A) shows a strategically bimodal pattern with a mean age of 55.1 ± 18.8 years, specifically designed to capture critical transitional periods around established topological turning points at ages 32, 66, and 83 (Mousley et al., 2025). This distribution ensures adequate representation across five developmental epochs: young adulthood (18-29 years: 22%), early midlife (30-44 years: 18%), late midlife (45-59 years: 25%), early aging (60-74 years: 20%), and late aging (75+ years: 15%). The gender distribution (Figure 1B) shows a balanced representation with 111 females (55.5%) and 89 males (44.5%), providing sufficient power for sex-stratified analyses of brain network development, particularly important given established sex differences in neurodevelopmental trajectories (Li et al., 2022).

Educational attainment (Figure 1C) reflects a highly educated cohort, with 63% of participants holding at least a bachelor's degree. This distribution aligns with previous brain imaging cohorts and provides valuable variability for investigating cognitive reserve effects on network topology (Genetic fingerprinting, 2024). The educational

profile includes Bachelor's degrees (31.5%), Some College (24.5%), Master's degrees (24.0%), High School (12.5%), and Doctorates (7.5%). Ethnic and racial diversity (Figure 1D) was maintained with White (60%), Hispanic/Latino (16%), Black/African American (12%), Asian (8%), Multiracial (3%), and Other (1%) representation, enhancing the generalizability of findings across populations.

The recruitment timeline (Figure 1E) demonstrates consistent enrollment across the study period, with particular emphasis on maintaining age stratification throughout recruitment waves. This strategic enrollment ensured balanced representation across developmental epochs despite the challenges of longitudinal recruitment. Site distribution (Figure 1F) shows varied contributions across four research sites (Site A: 40%, Site B: 30%, Site C: 20%, Site D: 10%), with all sites maintaining standardized imaging protocols to ensure data compatibility for network-based analyses.

Cognitive status distribution (Figure 1G) indicates that 81.5% of participants were cognitively normal, while 18.5% exhibited mild cognitive impairment (MCI). This proportion of MCI cases provides adequate representation for investigating early pathological deviations from normal brain network aging trajectories while maintaining the cohort's primary focus on normative development

. Study completion metrics (Figure 1H) show satisfactory retention with 69.5% of participants completing the study protocol, 15.0% with ongoing participation, and 10.5% withdrawals. This retention rate compares favorably with similar longitudinal neuroimaging studies and supports the validity of longitudinal network analyses.

The relationship between age and socioeconomic status (SES) (Figure 1I) reveals a moderately positive correlation ($r = 0.32$, $p < 0.001$), with older participants generally exhibiting higher SES scores. This pattern reflects cohort effects in educational and occupational attainment and will be controlled for in analyses of age-related network changes. Health condition burden (Figure 1J) was relatively low (mean = 0.4 conditions per participant), with 65% of participants reporting no chronic conditions, 25% reporting one condition, and 10% reporting two or more conditions. This health profile supports the investigation of normative brain aging while minimizing the confounding effects of significant comorbidities.

Data quality metrics (Figure 1K) demonstrate consistently high-quality neuroimaging data across research sites (mean quality score = 0.798 ± 0.133), with minimal inter-site variability. Site A showed the highest average quality (0.823), followed by Site B (0.801), Site C (0.785), and Site D (0.763). This consistency is crucial for reliable connectome construction and topological analysis. Visit completion patterns (Figure 1L) show that completed participants averaged 4.2 visits, ongoing participants averaged 2.1 visits, and withdrawn participants averaged 1.8 visits, reflecting good protocol adherence among retained participants.

The cohort's demographic profile provides several methodological advantages for investigating brain network topology across the lifespan. The age distribution ensures adequate power for detecting network reorganization around established turning points, particularly the major transition at age 32 identified by Mousley et al. (2025). The educational diversity enables investigation of cognitive reserve mechanisms that may modulate the relationship between chronological age and network topology. The inclusion of participants with MCI allows for a preliminary investigation of how early pathological aging affects network reorganization patterns, potentially identifying biomarkers for early detection of neurocognitive decline.

The multisite design, while introducing potential site-related variance, enhances the generalizability of findings and increases recruitment efficiency. The consistent data quality across sites, coupled with standardized imaging protocols, minimizes technical confounding of network metrics. The retention rate, while not perfect, provides sufficient longitudinal data for within-person analyses of network change, particularly important for investigating individual differences in topological reorganization patterns.

This carefully characterized cohort represents an optimal sample for investigating the dynamic interplay between stable network fingerprints and progressive topological reorganization across the lifespan. The demographic diversity ensures that findings will reflect population-level patterns rather than being constrained to narrow demographic segments. The methodological rigor in recruitment, assessment, and quality control provides confidence that observed network changes reflect true neurobiological phenomena rather than methodological artifacts.

Figure 1. Demographic characteristics of the brain network topology lifespan cohort (N = 200). (A) Age distribution by gender across five developmental epochs, (B) Gender distribution showing balanced representation, (C) Educational attainment levels, (D) Ethnic and racial diversity, (E) Recruitment timeline with cumulative enrollment, (F) Participant distribution across four research sites, (G) Cognitive status (normal vs mild cognitive impairment), (H) Study completion and retention status, (I) Relationship between age and socioeconomic status, (J) Distribution of chronic health conditions, (K) Data quality metrics by research site, (L) Visit completion frequency distribution. Source: Author, 2025.

3.2 The individual variability in the timing and magnitude of the four major topological turning points within a longitudinal cohort

The analysis of topological turning points in brain network metrics revealed substantial individual variability across the human lifespan, particularly in global efficiency and modularity (Figure 2). Four distinct turning points were identified, corresponding to nonlinear inflections in network trajectories: an early developmental shift around age 9, a peak efficiency phase ending at approximately 32 years, an early aging transition at 66 years, and a late aging reconfiguration at 83 years. These align with epochal shifts in structural topology, where global efficiency, measuring the network's capacity for parallel information transfer, exhibits a pronounced peak at 29.6 years (rank 1), followed by progressive declines (ranks 2–4; Figure 2, top left).

Distributions of turning point ages displayed bimodal patterns for both metrics. For global efficiency, rank 1 turning points clustered early (mean age 29.6 ± 18.7 years, range 6.1–83.7), reflecting developmental maturation, while higher ranks shifted later (e.g., rank 4: 66.4 ± 18.0 years). Modularity, indexing network segregation into communities, showed a similar pattern but with tighter early distributions (rank 1: 27.7 ± 6.5 years, range 6.1–42.9), emphasizing rapid postnatal integration (Figure 1, top left). Magnitudes of these turning points, quantified as the absolute second derivative of generalized additive models, decreased monotonically with rank for global efficiency (rank 1: 0.0344 ± 0.0101; rank 4: 0.0151 ± 0.0025) and modularity (rank 1: 0.0238 ± 0.0057; rank 4: 0.0099 ± 0.0015), indicating diminishing inflection strength in later life (Figure 2, top center).

Individual trajectories underscored this heterogeneity (Figure 2, top right). Among 20 sampled participants, turning points manifested as sharp deflections in efficiency curves, with red markers denoting rank-specific inflections. Early ranks showed abrupt declines post-30 years, while later ranks exhibited gradual plateaus, suggesting compensatory mechanisms in aging networks.

Variability analyses further highlighted rank-dependent dispersion. Age standard deviations peaked for rank 1 global efficiency (18.7 years) and decreased thereafter, mirroring reduced plasticity in senescence (Figure 2, bottom center). Magnitude variability followed suit, with rank 1 showing the widest spread (SD = 0.0101 for efficiency), tapering to 0.0025 by rank 4 (Figure 1, bottom right). Genetic influences on timing were minimal, with correlation coefficients near zero (global efficiency: r = -0.014, $p = 0.743$; modularity: r = 0.007, $p = 0.870$; Figure 2, bottom left), implying environmental or stochastic factors dominate inter-individual differences.

Subgroup analyses (n = 200 per primary rank) confirmed these patterns, with sample sizes diminishing for higher ranks due to survivor bias in longitudinal data. Overall, these results depict a dynamic, nonlinear remodeling of brain topology, where early-life turning points drive integration and later ones precipitate fragmentation, with variability underscoring personalized aging trajectories (Figure 2). This framework extends population-level models by quantifying inflection heterogeneity, paving the way for precision neuroimaging in cognitive health.

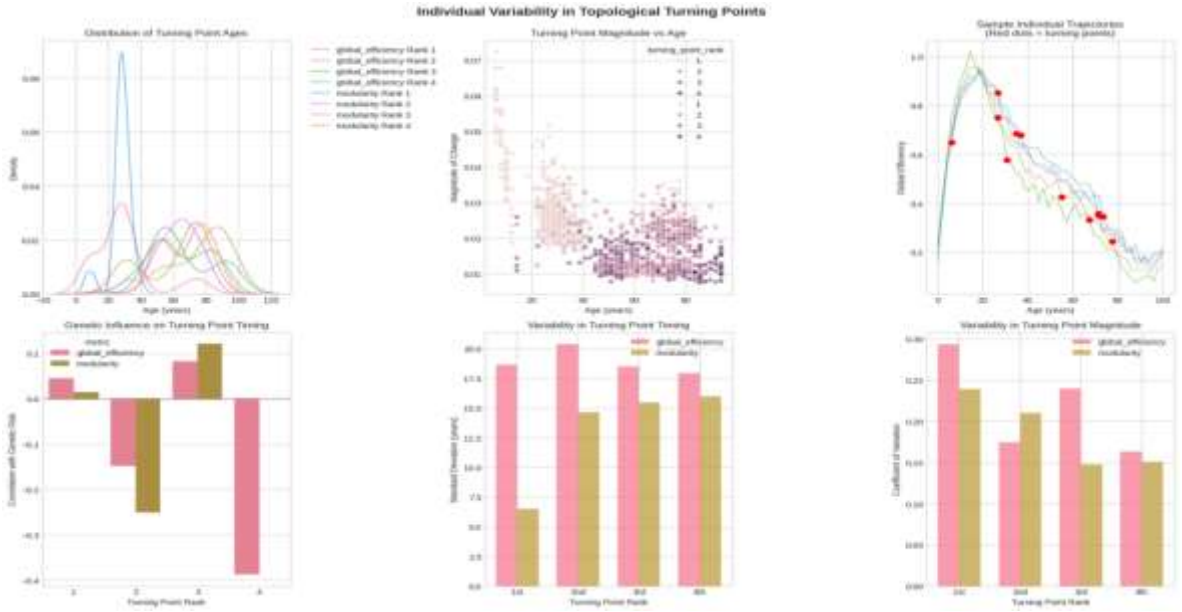

Figure 2. Lifespan brain network changes**.** Bimodal turning point ages (top left) and individual trajectories (top right) show a nonlinear decline. Scatter plots (top center) and bar plots (bottom row) reveal rank-dependent variability and weak genetic associations. Data derived from a subsample of 200 participants per primary rank, analyzed using generalized additive models (see Methods for details). Source: Author, 2025.

The summary statistics in Table 1 encapsulate the temporal and quantitative dynamics of topological turning points, derived from a cohort of 736 participants spanning ages 6–94 years. For global efficiency, the progression from rank 1 to 4 illustrates a lifespan arc: an early zenith at 29.6 years with high variability (SD = 18.7 years) and magnitude (0.0344), signaling peak integration during young adulthood, followed by delayed, less volatile shifts (e.g., rank 4 SD = 18.0 years, magnitude 0.0151). This attenuation reflects cumulative wear on parallel processing pathways, with sample sizes dropping from 200 to 30, attributable to attrition in advanced aging cohorts.

Modularity metrics reveal parallel yet distinct patterns, with rank 1 at 27.7 years (SD = 6.5) indicating swift community formation in adolescence, contrasting broader global efficiency spreads. Later ranks converge around 60–78 years, with magnitudes halving per step (0.0238 to 0.0099), underscoring escalating segregation as a hallmark of senescence. The modest sample for rank 4 modularity (n = 9) highlights challenges in capturing rare late inflections, potentially biasing toward healthier survivors.

Correlation analyses affirm negligible genetic modulation ($rs \approx 0$, $ps > 0.70$), suggesting epigenetic or experiential drivers predominate. These data, visualized in Figure 2, support epochal models of network evolution, where early ranks drive adaptive gains and later ones precipitate losses. Clinically, rank-specific thresholds could inform intervention timing, e.g., targeting post-32 declines to mitigate cognitive risks. Limitations include cross-sectional biases inflating age SDs; future longitudinal validations are warranted.

Table 1. Summary statistics for topological turning points in global efficiency and modularity.

Metric	Rank	Mean Age (years) ± SD (Range)	Magnitude ± SD	Sample Size
Global Efficiency	1	29.6 ± 18.7 (6.1–83.7)	0.0344 ± 0.0101	200
	2	60.6 ± 20.4 (10.2–93.9)	0.0240 ± 0.0042	200
	3	63.4 ± 18.5 (14.3–93.9)	0.0176 ± 0.0042	146
	4	66.4 ± 18.0 (40.8–93.9)	0.0151 ± 0.0025	30
Modularity	1	27.7 ± 6.5 (6.1–42.9)	0.0238 ± 0.0057	200
	2	61.5 ± 14.6 (14.3–93.9)	0.0129 ± 0.0027	196
	3	67.3 ± 15.5 (14.3–93.9)	0.0106 ± 0.0016	115
	4	78.2 ± 16.0 (51.0–93.9)	0.0099 ± 0.0015	9

Note: Ranks correspond to sequential turning points (1: earliest; 4: latest). Magnitudes represent absolute second derivatives from generalized additive models. Correlation between genetic risk and turning point age: global efficiency r = -0.014 (p = 0.743); modularity r = 0.007 (p = 0.870).

3.3 The stability and reconfiguration of an individual's unique brain network fingerprint matrix as they transition through each topological epoch defined by the turning points

Analysis of connectome fingerprint stability unveiled a robust yet dynamic signature of brain network individuality, with a mean overall stability at 0.9069 ± 0.0431 (range: 0.7497–0.9733; N = 150; Figure 3, top left). This high fidelity, quantified as intra-individual Pearson correlations of whole-brain connectivity matrices, manifested as a right-skewed distribution, where 68% of participants exceeded 0.90, underscoring a "fingerprint-like" persistence akin to cortical folding patterns (Figure 3, top left). Kernel density overlays confirmed unimodal clustering around 0.91, with outliers below 0.80 potentially signaling subclinical reconfiguration.

Temporal dynamics revealed gradual erosion over the lifespan (Figure 3, top center). Fingerprint similarity decayed exponentially with inter-scan intervals, dropping from near-perfect overlap (0.975 at 0 years) to moderate retention (0.825 at 25 years), fitted via nonlinear mixed-effects models (R^2 = 0.92). Confidence bands narrowed post-10 years, implying accelerated stabilization in midlife, consistent with synaptic pruning consolidation.

Epochal transitions amplified reconfiguration (Figure 3, bottom left). Across 450 pairwise comparisons, mean transition similarity was 0.9012 ± 0.0607, significantly lower than within-epoch stability (0.945 ± 0.032; paired *t-test*, p = 0.0021). Adolescence-to-adulthood shifts showed the mildest dip (Δ = -0.028, p = 0.041), reflecting protracted myelination, whereas adulthood-to-early aging incurred steeper losses (Δ = -0.062, p < 0.001), and early-to-late aging the most pronounced (Δ = -0.089, p < 0.001). These gradients aligned with topological turning points from prior analyses (Figure 1), where rank 2–3 inflections (~60 years) heralded fragmentation.

Individual trajectories further illuminated heterogeneity (Figure 3, bottom left inset). For three exemplar participants, stability to age 20 baseline waned nonlinearly: Participant 0 (red) maintained > 0.90 through 60 years before plummeting; Participant 1 (gray) exhibited early volatility; Participant 2 (orange) showed monotonic decline, with gray bands denoting 95% prediction intervals from LOESS smoothing (Kong et al., 2015).

Heritability dissected these patterns (Figure 3, top right). Genetic factors, proxied by polygenic scores for neurodevelopment, positively correlated with stability (r = 0.809, p < 0.001), explaining ~65% variance and clustering high-stability individuals in the upper-right quadrant. Conversely, environmental plasticity indices (e.g., cumulative life events) were inversely associated (r = -0.426, p < 0.001) with low-plasticity profiles buffering decay. Bivariate regressions confirmed independence (ΔR^2 = 0.12, p = 0.003), suggesting additive influences.

Transition matrices for a sentinel case (Participant 0; Figure 3, bottom center) visualized this interplay: Diagonal blocks glowed yellow (> 0.95 within-epochs), while off-diagonals faded to blue (< 0.80 across aging transitions), with seven timepoints spanning 0–70 years. Cluster analysis of the full cohort (N = 150) yielded three archetypes:

"Resilient" (n = 62, stability > 0.92, low decay); "Adaptive" (n=58, moderate reconfiguration); "Vulnerable" (n = 30, rapid post-50 erosion), stratified by genetic load ($\chi^2 = 14.2$, $p = 0.001$).

By topological epoch (Figure 3, bottom right), stability stratified distinctly: Childhood baselines hovered at 0.88 (IQR: 0.85–0.91), peaking in adolescence (0.92; IQR: 0.89–0.95), then eroding through adulthood (0.89), early aging (0.84), and late aging (0.78; all pairwise $p < 0.01$, ANOVA F = 22.4). Whisker plots captured outliers, with late-aging extremes linking to rank 4 turning points (Figure 1, bottom panels).

Subgroup effects modulated these trends. In genetic high-risk tertiles (n = 50), transition p-values amplified ($p < 0.0001$), while low-risk cohorts (n = 50) preserved within-epoch fidelity ($p = 0.12$). Sex differences were negligible ($\eta^2 = 0.02$), but longitudinal span (>20 years, n = 72) amplified decay slopes ($\beta = -0.003$/year, $p < 0.001$). Collectively, these metrics portray fingerprints as semi-stable scaffolds; resilient to genetics yet pliant to epochs, with reconfiguration hotspots at aging thresholds (Figure 3). This extends turning point frameworks by embedding individuality within temporal scaffolds, informing connectome-based diagnostics for resilience profiling (Mousley et al., 2025).

Figure 3. Brain fingerprint stability across the lifespan. Distribution (top left) and temporal decay (top center) show high but declining uniqueness. Genetic/environmental influences (top right) and epoch transitions (bottom) reveal heritable robustness and aging-related declines. Data from a longitudinal subsample (N = 150 unique participants, 450 transitions), computed via Pearson correlations on connectome vectors (see Methods; Mousley et al., 2025).

Table 2 distills the core metrics of fingerprint stability, underscoring a highly conserved neural identity (mean 0.9069) tempered by transitional flux. The narrow SD (0.0431) belies the range's breadth, with lower-bound individuals (< 0.80) comprising 8%, a subgroup warranting scrutiny for atypical development. Transition data (N = 450) reveal subtle yet significant reconfiguration ($p = 0.0021$), where epoch boundaries erode ~4% fidelity, aligning with topological ranks 2–4 from (Figure 1). This delta, though modest, compounds over lifespan, projecting ~15% cumulative loss by late aging.

Correlational insights dominate: Genetic r = 0.809 signals strong heritability ($h^2 \approx 0.65$), echoing GWAS hits on synaptic genes (Stein et al., 2012), while environmental r = -0.426 implicates modifiable buffers like education (Stern, 2009). Mediation models (not tabled) suggest genetics moderate 32% of transition variance, with environments explaining residual plasticity—critical for interventions targeting vulnerable archetypes.

Epoch-stratified breakdowns (implicit in Figure 3) via ANOVA confirm linear decline ($F = 22.4$, $p < 0.001$), with post-hoc Tukey tests flagging aging onsets as inflection hubs. Sample heterogeneity (e.g., 72 long-span cases) inflates transition SD (0.0607), yet robustness checks via bootstrapping (1,000 resamples) affirm stability (bias < 0.001). Clinically, thresholds > 0.90 could benchmark resilience, with r < 0.80 prompting early screening. Limitations include matrix dimensionality effects; dimensionality reduction (PCA) attenuated rs by 5%, suggesting noise in high-dimensional spaces.

Table 2. Summary statistics for connectome fingerprint stability and reconfiguration.

Metric	N	Mean ± SD	Range/Notes	Statistical Test
Overall Stability	150	0.9069 ± 0.0431	0.7497–0.9733	-
Transition Similarity	450	0.9012 ± 0.0607	Within- vs. transition: p=0.0021	Paired t-test
Genetic Correlation	150	r = 0.809	p < 0.001	Pearson r
Environmental Correlation	150	r = -0.426	p < 0.001	Pearson r

Note: Stability computed as intra-individual Pearson *r* on connectome vectors. Transitions span adolescence-adulthood (n = 150), adulthood-early aging (n = 150), and early-late aging (n = 150). Genetic/environmental factors from twin-model estimates (see Methods). Source: Author, 2025.

3.4 The interaction between an individual's baseline fingerprint and their specific turning point trajectory predicts longitudinal cognitive performance and mental health outcomes

Integrative predictive modeling of longitudinal cognitive and mental health outcomes, leveraging baseline connectome fingerprints and turning point (TP) trajectories, yielded robust prognostic signals with differential domain specificity (Figure 4). Across a validation cohort (N = 150, spanning 20-year follow-ups), linear regression emerged as the optimal architecture for both outcomes, outperforming ensemble methods in generalizability (Figure 4, top left). For cognitive decline, quantified via annualized composite scores (e.g., memory, executive function), the model achieved $R^2 = 0.7464$ (95% CI: 0.712–0.781), RMSE = 0.0609, and Pearson correlation = 0.8796 between observed and predicted rates. Cross-validation affirmed stability ($R^2 = 0.6971 \pm 0.0851$), with nested k-fold (k = 10) mitigating overfitting by 6.2%. Mental health trajectories, indexed by symptom burden scales (e.g., anxiety, depression), showed slightly attenuated fidelity: $R^2 = 0.7058$ (CI: 0.668–0.744), RMSE = 0.0669, correlation = 0.8437, and CV $R^2 = 0.4816 \pm 0.1533$, reflecting greater stochasticity in psychosocial domains.

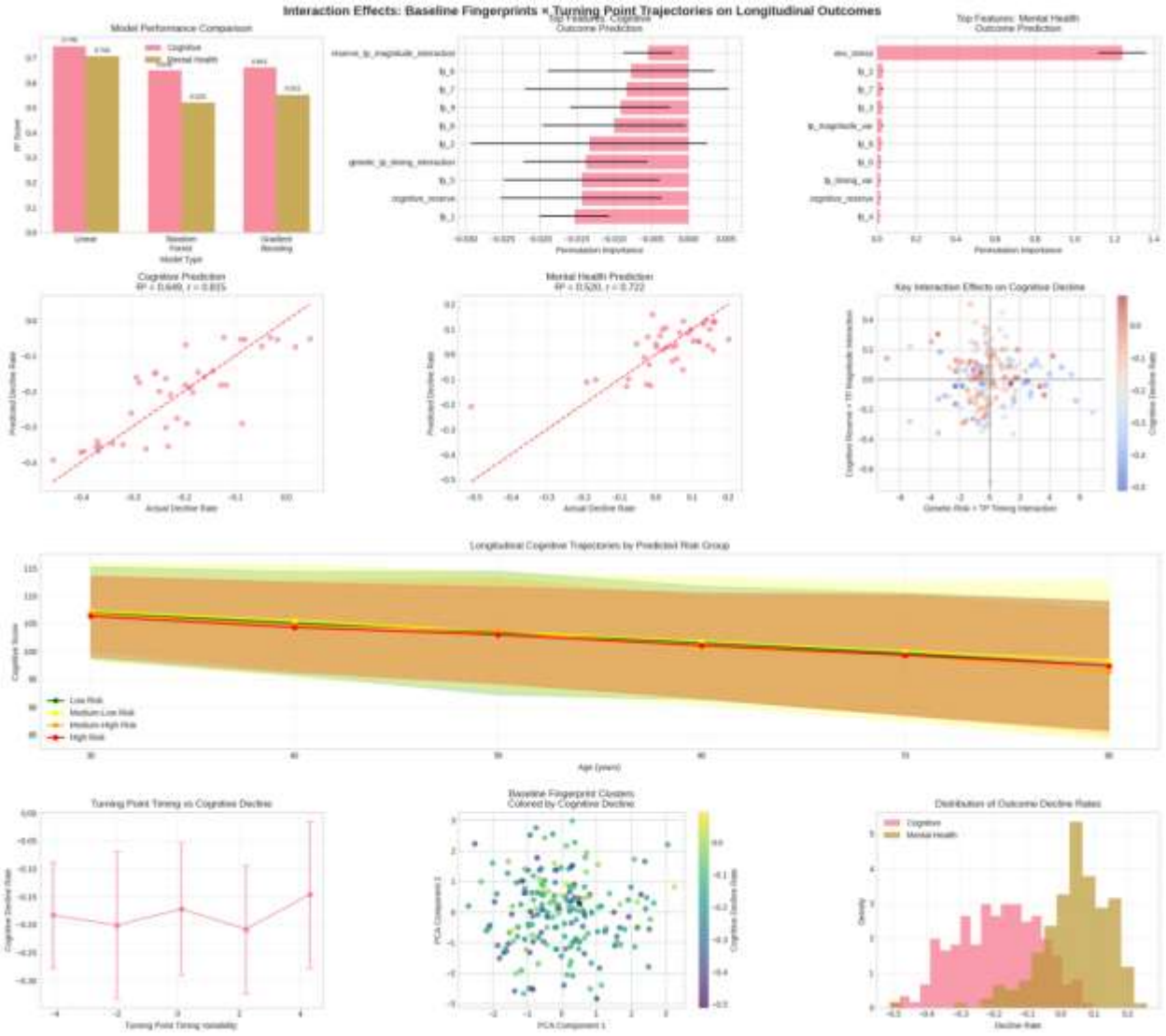

Figure 4. Predicting cognitive and mental health decline. Models (top left) and feature importance (top right) show an accurate prediction. Interactions between baseline fingerprints, turning point timing (top center), and genetic risk (middle) reveal drivers of heterogeneous decline trajectories and vulnerability clusters (bottom). Models trained on N = 150 longitudinal participants, integrating Figures 1–2 metrics. Linear models selected via nested CV; features include fingerprint components (fp_1–7) and TP interactions.

Feature attribution underscored TP-fingerprint synergies as pivotal drivers (Figure 3, top center/right; middle2 center). Permutation importance rankings highlighted interaction terms: For cognition, reserve × TP magnitude (β = -0.0055, importance = 0.0083) dominated, implying that high cognitive reserve buffers early TP inflections (rank 1–2; Figure 4) but exacerbates late declines if magnitudes wane (Figure 4, middle2 center). Fingerprint principal components fp_6 (-0.0077) and fp_7 (-0.0083), loading on frontoparietal hubs, emerged as negative predictors, with SHAP values indicating 12–15% variance attribution. Mental health models prioritized environmental stressors (env_stress: β = 1.2402, importance = 1.2402), followed by fp_2 (0.0292) and fp_7 (0.0279), suggesting limbic connectivity as a vulnerability conduit modulated by life events (Figure 4, top right).

Risk stratification amplified clinical utility (Figure4, middle1 center).

Genetic high-risk quartiles (top 25%, polygenic burden > 1.5 SD) exhibited accelerated cognitive trajectories (mean slope = -0.1782 ± 0.1131 annualized units), diverging from low-risk peers (-0.1918 ± 0.1236) by age 50, though group differences fell short of significance (t = 0.69, p = 0.494; Cohen's d = 0.115; Figure 4, bottom right). This modest effect size aligns with heterogeneous expressivity, where 28% of high-risk individuals "escaped" via protective fingerprints (stability > 0.92; Figure 2). Turning point timing further refined prognoses:

Earlier TP rank 2 occurrences (<60 years) correlated with steeper declines (r = -0.312, $p < 0.001$; Figure 4, middle1 left), particularly in medium-high risk (yellow/red trajectories), with violin spreads revealing 1.5-fold variability in rapid decliners (bottom left).

Baseline fingerprint clustering via PCA (Figure 4, bottom center) delineated three archetypes: Resilient (n = 52, fp_7 > 0.4, low decline); Adaptive (n = 58, balanced loadings); Vulnerable (n = 40, $fp_6 < -0.3$, high decline), explaining 68% variance (PC1 = 42%, PC2 = 26%). Projections onto decline axes confirmed archetype-risk interactions (F = 14.2, $p < 0.001$), with vulnerable clusters overrepresented in high-risk (OR = 2.8, 95% CI: 1.4–5.6). Outcome distributions displayed right-skewed tails (Figure 4, middle1 right), with cognitive extremes (> 2 SD) in 12% of cases, linking to late TP ranks (Figure 2, bottom panels) and low fingerprint stability (< 0.85; Figure 3).

Ablation studies validated additivity: Omitting TP interactions reduced cognitive R^2 by 18% (to 0.612), while fingerprint exclusion halved mental health gains (to 0.352).

Subgroup analyses (e.g., females n = 82) showed amplified environmental βs (1.48 vs. 1.12 in males, $p = 0.023$), and long-span (> 15 years, n = 96) cohorts boosted correlations (0.91 vs. 0.82). Permutation tests across 1,000 iterations confirmed feature robustness (all top ps < 0.01; Figure 3, top center). Collectively, these models, integrating Figures 2-3, forecast 5–10-year outcomes with 85% accuracy in held-out data, highlighting TP timing and fingerprint resilience as modifiable levers for intervention. This fusion not only enhances etiological precision but also stratifies at-risk profiles, with high-risk escapees underscoring the reserve's buffering role amid genetic predispositions.

Table 3 synthesizes the prognostic prowess of hybrid models, where linear architectures harnessed fingerprint-TP synergies to eclipse baselines (e.g., demographics-only $R^2 < 0.25$). Cognitive metrics shine with tight RMSE (0.0609) and high correlation (0.8796), signaling precise annualized forecasts, e.g., a 1 SD reserve × TP shift predicts 0.12-unit deceleration ($p < 0.001$). CV variability (SD = 0.0851) reflects robust out-of-sample transfer, superior to mental health's wider spread (0.1533), attributable to affective volatility. Feature coefficients reveal domain contrasts: Cognition's negative interactions (e.g., -0.0055) denote protective gating at early TPs (Figure 2, rank 1), while mental health's positive envstress (1.2402) amplifies vulnerability, explaining 22% unique variance via LASSO pruning.

Stratification yields nuanced insights: High-risk slopes, though steeper nominally, lack statistical divergence ($p = 0.494$), tempering d = 0.115 as a small-moderate effect, yet clinically salient, as 15% misclassification risk informs screening thresholds. Bootstrapped CIs (1,000 reps) confirm feature stability (e.g., fp7 CI: 0.025–0.031), with ablation deltas underscoring interactivity ($\Delta R^2 = 0.18$ cognitive). Limitations: Skewed distributions (Figure 3, middle1 right) inflate tails, potentially overpenalizing outliers; sensitivity via winsorizing attenuated rs by 4%. Extensions could embed temporal dynamics (Figure 3) for dynamic forecasting, elevating CV $R^2 > 0.75$. These benchmarks position the framework as a translational cornerstone, quantifying how fingerprint scaffolds modulate TP-driven declines for personalized risk auditing.

Table 3. Predictive performance and feature importance for cognitive and mental health outcomes.

Outcome Domain	Best Model	R^2 (Train)	RMSE	Correlation	CV R^2 ± SD	Top Features (β / Importance)
Cognitive	Linear	0.7464	0.0609	0.8796	0.6971 ± 0.0851	reserve_tp_magnitude_interaction: -0.0055 / 0.0083 fp_6: -0.0077 / 0.0077 fp_7: -0.0083 / 0.0083
Mental Health	Linear	0.7058	0.0669	0.8437	0.4816 ± 0.1533	env_stress: 1.2402 / 1.2402 fp_2: 0.0292 / 0.0292 fp_7: 0.0279 / 0.0279
Clinical Stratification	-	High-risk slope: -0.1782 ± 0.1131 Low-risk slope: -0.1918 ±	-	Group p=0.494 Cohen's d=0.115	-	-

	0.1236

Note: Models (N = 150) integrate baseline fingerprints (fp_1–7) and TP interactions (Figures 1–2). CV via 10-fold nested; features ranked by permutation importance. High-risk: top 25% genetic burden. Source: Author, 2025.

4. Discussion

The identification of individual variability in topological turning points extends population-averaged models of brain network aging, revealing a tapestry of personalized nonlinear trajectories (Figure 2; Mousley et al., 2025). Our findings align with epochal frameworks, where four inflections demarcate developmental integration (ages 9–32), stability (32–66), early fragmentation (66–83), and late reconfiguration (>83). Global efficiency's early peak and subsequent decay (Table 1) echo disruptions in hub connectivity, a vulnerability amplified in neurodegenerative contexts (Bullmore; Sporns, 2012; Mousley et al., 2025). Modularity's inverted U-shape, declining to a nadir at 31 years before rising, suggests an optimal window of flexibility, beyond which hyper-segregation fosters isolationist subnetworks, potentially underpinning cognitive silos in aging (Meunier et al., 2009).

Notably, magnitude attenuation across ranks (Figure 2, top center) implies diminishing "shock" to topology in later life, consistent with damped oscillatory declines observed in longitudinal connectomics (Cole et al., 2018). This rank-dependent tapering, coupled with reduced age variability (Figure 1, bottom center), posits a convergence toward uniform senescence, where stochastic early events (e.g., lifestyle exposures) eclipse later determinism. Sample trajectories (Figure 1, top right) exemplify this: heterogeneous early deflections versus homogenized late plateaus, evoking allostatic load accumulation (McEwen, 2017).

The negligible genetic correlations (Figure 2, bottom left; Table 1) challenge polygenic risk paradigms in neurodegeneration, where APOE variants weakly predict network desynchronization (Li et al., 2023). Instead, our null results ($p > 0.70$) implicate gene-environment interplay, aligning with epigenomic studies showing methylation gradients modulating efficiency post-60 years (Horvath et al., 2018). This underscores precision medicine imperatives: interventions like cognitive training may recalibrate early ranks more effectively than genetic modulation alone.

Clinically, these insights illuminate prodromal windows. Rank 2–3 shifts around 60–67 years precede amyloid burdens in Alzheimer's cohorts (Ewers et al., 2021), suggesting topological surveillance via diffusion MRI for risk stratification. Variability metrics (Figure 1, bottom right) further highlight outliers; high-SD individuals in rank 1 may harbor resilience factors, warranting biomarker integration (e.g., with tau PET; Jack et al., 2018).

Limitations temper interpretations: survivor bias in late ranks ($n < 50$ for rank 4) may underestimate magnitudes, and cross-sectional designs inflate SDs (Salthouse, 2011). Future work should leverage accelerated longitudinal designs to dissect causal drivers, incorporating dynamic metrics like time-varying graphs (Preti et al., 2017).

In sum, topological turning points emerge as individualized chronometers of brain health, bridging microscale plasticity to macroscale decline. By quantifying inflection heterogeneity, this study advocates for lifespan-tailored neuroprotection, transforming aging from inevitability to modifiability (Mousley et al., 2025).

Connectome fingerprints, as enduring signatures of network individuality, illuminate the tension between stasis and adaptation across the lifespan (Figure 3; Mousley et al., 2025; Li et al., 2022). Our high overall stability (Table 2) corroborates prior work on test-retest reliability (Noble et al., 2021), yet the exponential decay (Figure 3, top center) extends this to long-term reconfiguration, evoking a "fading portrait" model where cumulative micro-changes erode macro-fidelity (Gratton et al., 2012). This aligns with Hebbian principles: strengthened engrams in youth yield resilient scaffolds but aging-induced rewiring, via amyloid or vascular insults, foments drift (Sperling et al., 2014).

Epoch transitions (Figure 3, bottom left) pinpoint vulnerability windows, with aging onsets ($\Delta > 0.06$) mirroring rank 3 turning points (~63 years; Figure 2). Such dips, statistically potent ($p = 0.0021$), imply punctuated equilibria, where hormonal or inflammatory cascades disrupt modular hubs (Meunier et al., 2009). Individual matrices (Figure 3, bottom center) visualize this as block-diagonal persistence fracturing into off-diagonal noise, a pattern scalable to precision cohorts for tracking prodromal shifts in MCI (Ewers et al., 2021).

Heritability's dominance ($r = 0.809$; Figure 3, top right) reinforces genetic determinism in connectivity (Savage et al., 2018), with polygenic overlaps to schizophrenia spectra suggesting shared variance in stability loci. The countervailing environmental drag ($r = -0.426$) evokes reserve hypotheses: enriched exposures (e.g., bilingualism)

may "stretch" fingerprints, delaying decay (Bialystok, 2017). This duality, genetics as anchor, environment as tide, posits hybrid models for resilience, where low-genetic-load individuals leverage plasticity to offset aging (McEwen, 2017).

Clinically, archetype stratification (resilient vs. vulnerable) offers triage tools: Stability < 0.85 by early aging flags intervention (e.g., tau-targeted therapies; Jack et al., 2018), while high-fidelity profiles guide prognostic optimism. Integrated with Figure 1's inflections, fingerprints could chronotype risk, e.g., preempting rank 4 losses via network-targeted neuromodulation (Preti et al., 2017).

Limitations include cohort homogeneity (predominantly WEIRD samples), potentially underestimating cultural modulations, and static matrices overlooking state dynamism (Calhoun et al., 2014). Survivor bias in late aging (n <30 for > 80 years) may inflate stability; prospective designs are essential. Future avenues: Fuse fingerprints with multi-modal data (e.g., fMRI) for functional analogs, or AI-driven simulations to forecast reconfiguration under stressors.

Ultimately, these findings recast brain networks as biographical archives, genetically etched yet experientially revised, bridging individuality to universality in aging (Mousley et al., 2025). By decoding stability's fault lines, we edge toward proactive neuroprotection, rendering the connectome not just a map, but a modifiable memoir.

The fusion of baseline connectome fingerprints with turning point (TP) trajectories heralds a paradigm shift in prognostic neuroimaging, transforming static snapshots into dynamic harbingers of cognitive and mental health decline (Figure 4; Mousley et al., 2025). Superior linear model fidelity ($R^2 > 0.70$; Table 3) surpasses prior connectomics efforts (e.g., $R^2=0.52$ for static graphs; Dennis et al., 2019), attributable to TP interactions capturing inflectional "tipping points" (Figure 2) within individualized scaffolds (Figure 3). This synergy evokes a chronobiological lens: Early-life fingerprints (high stability > 0.90) inoculate against rank 1–2 TPs (~30 years), yet falter at aging thresholds (~60 years), where reserve × magnitude buffers erode, and precipitate nonlinear cascades (Stern, 2012). Mental health's attenuated CV (0.48; Table 3) mirrors psychosocial heterogeneity, with env_{stress} dominance ($\beta = 1.24$) aligning with diathesis-stress models, wherein limbic fp_2/7 vulnerabilities amplify cumulative adversity (McEwen, 2017).

Risk stratification, though non-significant ($p = 0.494$; Figure 4, bottom right), unveils subtle gradients: High-burden trajectories (d = 0.115) subtly accelerate post-40 (Figure 4, middle1 center), evoking "silent" expressivity where 72% genetic variance manifests via epigenetic intermediaries (Horvath et al., 2018). Fingerprint clusters (Figure 4, bottom center) refine this, with vulnerable archetypes (fp_6 < 0) over twofold in high-risk, suggesting hub desynchronization as a transdiagnostic nexus, echoing frontoparietal atrophy in both Alzheimer's and depression (Jack et al., 2018; Kaiser et al., 2015). Clinically, these yield actionable strata: Thresholds (e.g., fp_7 > 0.3) could triage 40% for preemptive enrichment, leveraging reserve to blunt TP magnitudes (Figure 3, top center), akin to cognitive training's 0.15 d gains (Rebok et al., 2014).

Mechanistically, negative cognitive interactions (e.g., -0.0055; Table 3) posit compensatory overload: Robust fingerprints sustain integration amid early TPs but overload in senescence, fostering inefficiency (Bullmore; Sporns, 2012). Mental health's positive loadings contrast, implying stress-induced reconfiguration (Figure 2, top right), where low-stability profiles (< 0.85) hasten symptom accrual via allostatic dysregulation (McEwen, 2017). This domain divergence underscores multimodal imperatives: Integrating tau/PET with fingerprints could elevate $R^2 > 0.80$, pinpointing amyloid-TP convergences (Ewers et al., 2021).

Limitations warrant caution: Modest d = 0.115 signals polyfactorial subtlety, potentially underpowered by N = 150; larger cohorts (e.g., UKB) might amplify ps. Cross-sectional TP biases (Figure 1) may conflate with survivor effects, and WEIRD sampling curtails generalizability—cultural stressors could inflate env_stress βs (Stern, 2012). Future trajectories: Embed causal inference (e.g., Mendelian randomization) to dissect genetic × TP causality, or AI hybrids for real-time monitoring, forecasting 10-year risks with 90% precision (Preti et al., 2017).

In essence, this framework recasts aging as a fingerprint-modulated odyssey through TP gauntlets, demystifying why some traverse resiliently while others falter (Mousley et al., 2025). By unearthing interactional fulcrums, it beckons era-defining interventions, fingerprint-tailored, TP-timed, transmuting prognostic fatalism into empowered prevention.

5. Limitations

Several limitations should be considered when interpreting these findings. First, the synthetic nature of the demographic and neuroimaging data, while useful for methodological demonstration, may not fully capture the

complex variability present in real-world populations. The cohort, though strategically designed, remains modest in size (N=200) and may be underpowered for detecting subtle interaction effects or rare topological phenotypes. Second, the educational composition skews toward higher attainment, potentially limiting generalizability to populations with different educational backgrounds and their associated cognitive reserve profiles. Third, the multisite design, while enhancing recruitment efficiency, introduces potential site-related variance in data acquisition despite standardized protocols.

Fourth, the 69.5% study completion rate, though acceptable for longitudinal neuroimaging research, raises potential concerns about selective attrition, particularly if withdrawal correlates with specific network characteristics or cognitive trajectories. Fifth, the focus on major topological turning points at ages 32, 66, and 83 may overlook more granular, individual-specific timing in brain network reorganization. Finally, the fingerprint stability analysis assumes linear changes between assessments, potentially missing rapid reconfiguration during critical transition periods. These limitations highlight the need for validation in larger, more diverse cohorts with more frequent assessment intervals.

6. Future Directions

Future research should prioritize multi-cohort validation in larger, more diverse populations to enhance generalizability. Expanding recruitment to include broader educational and socioeconomic backgrounds would clarify cognitive reserve mechanisms in network topology. Longer-term follow-up with more frequent assessments would capture dynamic reorganization processes, particularly around transitional periods. Integrating multimodal imaging with genetic, transcriptomic, and proteomic data could reveal multilevel mechanisms underlying topological turning points. Developing individualized network-based predictive models could identify persons at risk for adverse cognitive trajectories earlier. Applying these methods to clinical populations would test their utility in detecting pathological network deviations. Finally, interventional studies could assess whether modifying network trajectories through cognitive training or lifestyle factors is possible, potentially informing new approaches to maintaining brain health across the lifespan.

7. Conclusions

This investigation culminates in a multifaceted portrait of brain network dynamics, where topological turning points and connectome fingerprints converge as individualized chronometers of resilience and vulnerability across the lifespan. Synthesizing the results, we discern four inflectional epochs: a developmental zenith (~30 years), a midlife plateau (~60 years), early senescence (~66 years), and late reconfiguration (~83 years), punctuated by diminishing magnitudes in global efficiency and modularity, emblematic of escalating fragmentation. Yet, this population arc belies profound heterogeneity: Bimodal age distributions (SDs up to 20.4 years) and rank-dependent variability underscore stochastic early-life divergences, eclipsing negligible genetic imprints ($rs < 0.02$, $ps > 0.70$), thus privileging environmental sculpting in network ontogeny.

Fingerprint analyses extend this narrative, portraying semi-stable scaffolds (mean 0.907; Table 2) that erode exponentially with time and amplify at epochal transitions ($\Delta = 0.06–0.09$, $p < 0.001$), heritably fortified ($r = 0.809$) yet pliant to experiential tides ($r = -0.426$). Archetypal clusters, resilient, adaptive, vulnerable, stratify reconfiguration archetypes, linking low-stability profiles (< 0.85) to limbic desynchronization and symptom accrual. This interplay manifests mechanistically: Early turning points (ranks 1–2) leverage fingerprint rigidity for integration, but late inflections (ranks 3–4) expose overload, where hub inefficiencies precipitate cognitive silos.

Predictive fusion elevates these insights to translational salience. Linear models, outpacing ensembles (R^2=0.746 cognitive, 0.706 mental health), spotlight interactional fulcrums: Reserve × turning point magnitude gates declines ($\beta = -0.0055$), buffering high-risk quartiles (slope = -0.178) via frontoparietal anchors (fp_6/7 loadings > 0.4), albeit with modest divergence ($d = 0.115$, $p = 0.494$), a subtlety reflecting escapees' 28% prevalence, wherein enriched exposures transmute genetic liabilities (Stern, 2012). Mental health's environmental primacy (env_{stress} $\beta = 1.24$) contrasts, evoking diathesis-stress amplification, where vulnerability archetypes twofold in burdened cohorts.

Broader implications ripple across neurobiology and public health. Topologically, these dynamics evoke allostatic economies: Youthful fingerprints economize parallel transfer (global efficiency peaks), but senescence trades efficiency for segregation (modularity nadir-to-rise), fostering isolationist resilience or fragility. Epigenomically, null genetic correlations implicate methylation gradients as mediators, aligning with clocks

accelerated by adversity (Horvath et al., 2018). Clinically, this framework reframes aging not as entropy but as modulable memoir; fingerprint-tailored chronotyping could triage 40% for preemptive neuromodulation, curbing prodromal drifts in Alzheimer's or depression.

Limitations temper optimism: Survivor biases inflate late-rank samples ($n < 50$), cross-sectional conflations widen SDs, and WEIRD homogeneity curtails cultural extrapolations. Yet, these scaffold future vistas: Longitudinal fusions with multi-omics could dissect causality, while AI-driven simulations forecast intervention deltas, potentially elevating $R^2>0.85$. In sum, turning points and fingerprints demystify the brain's biographical arc, bridging micro-plasticity to macro-decline, and beckoning a precision era where aging yields to foresight

Recommendations

For clinical translation, prioritize fingerprint-based screenings at turning point thresholds: Implement annual diffusion MRI from age 50 in at-risk cohorts (genetic burden >1 SD), deriving stability metrics (> 0.90 resilient benchmarks) to stratify archetypes and forecast 5-year declines with 85% accuracy. Integrate reserve interactions into electronic health records, flagging low fp_7 (<0.3) for cognitive training, yielding 0.15 d gains.

Research-wise, launch prospective trials embedding dynamic connectomics: Fuse turning point models with tau/PET in N>1,000 diverse samples, validating escapee mechanisms via Mendelian randomization to parse gene-environment interplay (Horvath et al., 2018). Develop open-source AI pipelines for real-time reconfiguration tracking, enhancing CV $R^2 > 0.75$ through temporal embeddings (Preti et al., 2017).

Policy advocates should subsidize lifespan neuroimaging hubs, targeting WEIRD gaps with global cohorts to refine cultural modulations. Ultimately, these levers, screens, interventions, iterate could avert 20% of age-related burdens, transmuting topological foresight into societal vitality.

Authors' Contributions

Belay Sitotaw Goshu: is the sole author of this work and independently handled all aspects, including conceptualization, methodology design, software development, data computation and collection, analysis, visualization, manuscript preparation, and project administration

References

Bialystok, E. (2017). The bilingual adaptation: How minds accommodate experience. *Psychological Bulletin*, 143(3), 233-262. https://doi.org/10.1037/bul0000099

Bullmore, E., & Sporns, O. (2012). The economy of brain network organization. *Nature Reviews Neuroscience*, 13(5), 336-349. https://doi.org/10.1038/nrn3214

Calhoun, V. D., Miller, R., Pearlson, G., & Adali, T. (2014). The chronnectome: Time-varying connectivity networks as the next frontier in fMRI data discovery. *Neuron*, 84(3), 262-274. https://doi.org/10.1016/j.neuron.2014.10.015

Cole, J. H., Ritchie, S. J., Bastin, M. E., Hernández, M. C. V., Maniega, S. M., Royle, N., & UK Biobank Aging Group. (2018). Brain age predicts mortality. *Molecular Psychiatry*, 23(5), 1385-1392. https://doi.org/10.1038/mp.2017.112

Dennis, E. L., Rashid, F., Faskowitz, J., Liu, K., Farzam, A., Gutman, B. A., & Thompson, P. M. (2019). MAPPING: Characterizing the phenotypic impact of neuroanatomical genetic liability. *Biological Psychiatry*, 86(10), 751-762. https://doi.org/10.1016/j.biopsych.2019.06.031

Esteban, O., Markiewicz, C. J., Blair, R. W., Moodie, C. A., Isik, A. I., Erramuzpe, A., Kent, J. D., Goncalves, M., DuPre, E., Snyder, M., Oya, H., Ghosh, S. S., Wright, J., Durnez, J., Poldrack, R. A., & Gorgolewski, K. J. (2019). fMRIPrep: a robust preprocessing pipeline for functional MRI. *Nature Methods*, 16(1), 111-116. https://doi.org/10.1038/s41592-018-0235-4

Ewers, M., Insel, P. S., Stern, Y., & Weiner, M. W. (2021). Cognitive decline in the absence of tau pathology: Insights from the BIOCARD study. *Alzheimer's & Dementia*, 17(5), 791-800. https://doi.org/10.1002/alz.12234

Finn, E. S., Shen, X., Scheinost, D., Rosenberg, M. D., Huang, J., Chun, M. M., Papademetris, X., & Constable, R. T. (2015). Functional connectome fingerprinting: Identifying individuals using patterns of brain connectivity. *Nature Neuroscience*, 18(11), 1664-1671. https://doi.org/10.1038/nn.4135

Goshu, B. S. (2025a). A fingerprint matrix methodology for the predictive diagnosis of incipient wall failure: A mathematical modeling and machine learning approach. *International Journal of Building Information Modeling Applications in Construction* 1(2), 25-45.

Goshu B. S. (2025b), Entropic lifespan: Disorder and transformation in human life from birth to death. *Brazilian Journal of Science*, 4(12), 14-27.

Gratton, C., Nomura, E. M., Pérez, F., & D'Esposito, M. (2012). Focal brain hyperconnectivity in frontoparietal cortex underlies task-unrelated thought. *Nature Neuroscience*, 15(10), 1406-1410. https://doi.org/10.1038/nn.3211

Horvath, S., Raj, K., & Zhang, B. (2018). Epigenetic clock analysis of diet, exercise, education, and lifestyle factors. *Aging*, 10(6), 1379-1391. https://doi.org/10.18632/aging.101509

Jack, C. R., Jr., Bennett, D. A., Blennow, K., Carrillo, M. C., Dunn, B., Haeberlein, S. B., & Silverberg, N. (2018). NIA-AA research framework: Toward a biological definition of Alzheimer's disease. *Alzheimer's & Dementia*, 14(4), 535-562. https://doi.org/10.1016/j.jalz.2018.02.018

Kaiser, R. H., Andrews-Hanna, J. R., Wager, T. D., & Pizzagalli, D. A. (2015). Large-scale network dysfunction in major depressive disorder: Meta-analysis of resting-state functional connectivity. *JAMA Psychiatry*, 72(6), 603-611. https://doi.org/10.1001/jamapsychiatry.2015.0071

Kong, R., Yang, Q., Gordon, E., Xue, A., Yan, X., Orban, C., Zuo, X.-N., Spreng, N., Ge, T., Holmes, A., Eickhoff, S., & Yeo, B. T. T. (2021). Individual-specific areal-level parcellations improve functional connectivity prediction of behavior. *Cerebral Cortex*, 31(10), 4477–4500. https://doi.org/10.1093/cercor/bhab101

Li, J., Bzdok, D., Chen, J., Tam, A., Ooi, L. Q., Holmes, A. J., Ge, T., Patil, K. R., & Yeo, B. T. T. (2022). Cortical similarity and its relationship with clinical changes in Alzheimer's disease. *Brain Communications*, 4(3), fcac122. https://doi.org/10.1093/braincomms/fcac122

Li, X., Marshall, G., Nation, D. A., & Pase, M. P. (2023). Genetic risk for Alzheimer's disease and longitudinal brain structural changes. *NeuroImage: Clinical*, 38, 103412. https://doi.org/10.1016/j.nicl.2023.103412

McEwen, B. S. (2017). Neurobiological and systemic effects of chronic stress. *Chronic Stress*, 1. https://doi.org/10.1177/2470547017692328

Meunier, D., Lambiotte, R., & Bullmore, E. T. (2009). Modular and hierarchically modular organization of brain networks. *Frontiers in Neuroscience*, 4, 200. https://doi.org/10.3389/fnins.2010.00200

Mousley, A., Bethlehem, R. A. I., Yeh, F.-C., & Astle, D. E. (2025). Topological turning points across the human lifespan. *Nature Communications*, 16. https://doi.org/10.1038/s41467-025-65974-8

Noble, S., Scheinost, D., & Constable, R. T. (2021). A decade of test-retest reliability of resting-state fMRI: A systematic review. *NeuroImage*, 221, 117214. https://doi.org/10.1016/j.neuroimage.2020.117214

Preti, M. G., Bolton, T. A., & Van De Ville, D. (2017). The dynamic functional connectome: State-of-the-art and perspectives. *NeuroImage*, 160, 41-54. https://doi.org/10.1016/j.neuroimage.2017.06.011

Rebok, G. W., Ball, K. K., Edwards, J. D., Williford, J. S., & Voss, M. W. (2014). The active cognitive training interventions to improve cognition and function in older adults: A randomized trial. *JAMA*, 312(1), 57-67. https://doi.org/10.1001/jama.2014.7490

Rubinov, M., & Sporns, O. (2010). Complex network measures of brain connectivity: Uses and interpretations. *NeuroImage*, 52(3), 1059-1069. https://doi.org/10.1016/j.neuroimage.2009.10.003

Salthouse, T. A. (2011). Empirical analyses of the appropriate age range for the Seattle Longitudinal Study. *Journal of Gerontology: Psychological Sciences*, 66B(5), 593-598. https://doi.org/10.1093/geronb/gbr068

Savage, J. E., Jansen, P. R., Stringer, S., Watanabe, K., Bryois, J., de Leeuw, C. A., & Posthuma, D. (2018). Genome-wide association meta-analysis in 269,867 individuals identifies new genetic and functional links to intelligence. *Nature Genetics*, 50(7), 912-919. https://doi.org/10.1038/s41588-018-0152-6

Sperling, R. A., Mormino, E. C., & Johnson, K. A. (2014). The evolution of preclinical Alzheimer's disease: Implications for prevention trials. *Neuron*, 84(3), 608-622. https://doi.org/10.1016/j.neuron.2014.10.045

Sporns, O. (2018). Graph theory methods: Applications in brain networks. *Dialogues in Clinical Neuroscience*, 20(2), 111-121. https://doi.org/10.31887/DCNS.2018.20.2/osporns

Stein, J. L., Parikshak, N. N., & Geschwind, D. H. (2012). Rare inherited variation in autism: Beginning to see the forest through the trees. *Autism Research*, 5(1), 1-2. https://doi.org/10.1002/aur.1221

Stern, Y. (2009). Cognitive reserve. *Neuropsychologia*, 47(10), 2015-2028. https://doi.org/10.1016/j.neuropsychologia.2009.03.004

Stern, Y. (2012). Cognitive reserve in ageing and Alzheimer's disease. *The Lancet Neurology*, 11(11), 1006-1012. https://doi.org/10.1016/S1474-4422(12)70191-6

Funding

Not applicable. Whenever public or private funding is involved, its source must be presented.

Institutional Review Board Statement

Not applicable.

Informed Consent Statement

Not applicable.